nature neuroscience

A temporal basis for predicting the sensory consequences of motor commands in an electric fish

Ann Kennedy[1], Greg Wayne[1,3], Patrick Kaifosh[1,3], Karina Alviña[1], L F Abbott[1,2] & Nathaniel B Sawtell[1]

Mormyrid electric fish are a model system for understanding how neural circuits predict the sensory consequences of motor acts. Medium ganglion cells in the electrosensory lobe create negative images that predict sensory input resulting from the fish's electric organ discharge (EOD). Previous studies have shown that negative images can be created through plasticity at granule cell–medium ganglion cell synapses, provided that granule cell responses to the brief EOD command are sufficiently varied and prolonged. Here we show that granule cells indeed provide such a temporal basis and that it is well-matched to the temporal structure of self-generated sensory inputs, allowing rapid and accurate sensory cancellation and explaining paradoxical features of negative images. We also demonstrate an unexpected and critical role of unipolar brush cells (UBCs) in generating the required delayed responses. These results provide a mechanistic account of how copies of motor commands are transformed into sensory predictions.

Weakly electric mormyrid fish emit brief EOD pulses for communication and active electrolocation. However, the fish's own EOD also affects passive electroreceptors tuned to detect external fields. Previous studies have shown that such interference, a ringing pattern of activation that may persist for as long as the interval between EODs[1], is cancelled out in medium ganglion cells through the generation of motor corollary discharge responses that are temporally specific negative images of the sensory consequences of the EOD[2]. Elegant theoretical studies[3,4] have suggested that anti-Hebbian spike timing–dependent plasticity known to exist at synapses from granule cells onto medium ganglion cells[5] could provide a basis for formation of negative images, but this work depends on the untested assumption that granule cell corollary discharge responses exhibit a rich temporal structure spanning the ~200 ms during which negative images can be generated[2,6,7] (**Fig. 1a**). Granule cells, located in the eminentia granularis posterior (EGp) overlying the electrosensory lobe (ELL) molecular layer, receive excitatory input from extrinsic mossy fibers originating from neurons in several brain regions and from UBCs located in the EGp itself (**Fig. 1b**). Though there are a small number of published recordings of delayed corollary discharge responses from unidentified elements in the EGp itself[8], corollary discharge responses of mossy fibers appear to be extremely brief and minimally delayed, resembling literal copies of the EOD motor command[8–11]. Moreover, delayed or temporally diverse corollary discharge responses have not been reported for granule cells. Therefore, we set out to determine whether delayed and temporally diverse granule cell responses exist and, if they do, how they are generated and whether they are sufficient to support negative-image formation.

As in previous studies, we took advantage of an awake preparation in which fish continue to emit the motor command to discharge the electric organ but the EOD itself is blocked by neuromuscular paralysis, allowing corollary discharge responses, i.e., neural activity in sensory areas that is time-locked to the EOD motor command, to be studied in isolation from sensory effects.

RESULTS

Corollary discharge responses in mossy fibers and UBCs

Consistent with previous studies[8–11], extracellular recordings from two midbrain nuclei that are the main sources of corollary discharge input to granule cells revealed responses restricted to short delays after the EOD motor command (**Fig. 1c**; paratrigeminal command–associated nucleus, $n = 12$ recordings; preeminential nucleus, $n = 31$ recordings). To characterize corollary discharge inputs to granule cells, we used high-impedance glass microelectrodes to record from putative mossy fiber axons in the EGp itself (see Online Methods for details of mossy fiber recordings). Most mossy fibers recorded in the EGp exhibited responses restricted to short delays, termed early and medium, that closely resembled the responses recorded in midbrain neurons that send mossy fibers to the EGp (**Fig. 1d**,**e**; early, $n = 54$ recordings; medium, $n = 28$ recordings). Thus, corollary discharge inputs to the EGp appear to be insufficient for cancelling the effects of the EOD over its entire duration. However, we also found other putative mossy fibers in the EGp, termed late and pause, that exhibited far more delayed and diverse corollary discharge responses (**Fig. 1d**,**e**; late, $n = 26$ recordings; pause, $n = 27$ recordings). Late mossy fibers fired bursts or single action potentials at long delays after the EOD command (>50 ms). Pause mossy fibers showed highly regular tonic firing that ceased abruptly around the time of the command. Resumption of firing was often marked by precise time-locking of spikes at long delays relative to the EOD command (**Fig. 1d**).

A candidate for the source of late and pause responses recorded in the EGp are the UBCs that, as in the mammalian cerebellum and dorsal cochlear nucleus[12], give rise to an intrinsic system of mossy fiber axons that provides additional excitatory input to

[1]Department of Neuroscience, Columbia University, New York, New York, USA. [2]Department of Physiology and Cellular Biophysics, Columbia University, New York, New York, USA. [3]These authors contributed equally to this work. Correspondence should be addressed to N.B.S. (ns2635@columbia.edu).

Received 22 August 2013; accepted 16 January 2014; published online 16 February 2014; doi:10.1038/nn.3650

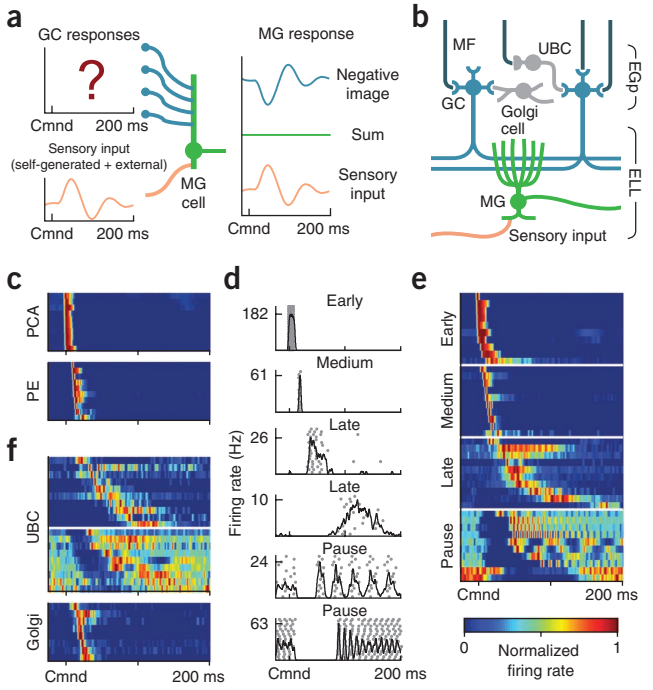

Figure 1 Corollary discharge responses in mossy fibers, UBCs and Golgi cells. (**a**) Schematic of negative image formation and sensory cancellation in a medium ganglion cell (MG). The question mark indicates that temporal patterns of corollary discharge response in granule cells (GCs) are the critical unknown in current models of sensory cancellation. Cmnd, EOD command. (**b**) Schematic of the circuitry of the EGp and ELL. Corollary discharge signals related to the EOD motor command are relayed via several midbrain nuclei (not shown) and terminate in EGp as mossy fibers (MF; black inputs from top). UBCs give rise to an intrinsic system of mossy fibers that provides additional excitatory input to granule cells. Golgi cells inhibit granule cells and UBCs. Medium ganglion cells in the ELL receive both sensory input and granule cell input via parallel fibers. (**c**) Corollary discharge responses of units recorded in the paratrigeminal command associated nucleus (PCA) and the preeminential nucleus (PE). Each row shows the smoothed (5 ms Gaussian kernel) average firing rate of a single unit normalized by its maximum firing rate. In this and subsequent panels time is defined relative to the EOD motor command (Cmnd), which is emitted spontaneously by the fish at 2–5 Hz. Color bar in **e** applies to **c** and **f**. (**d**) Example spike rasters (gray dots) and smoothed firing rates (black curves) for putative mossy fibers recorded extracellularly in the EGp, illustrating four temporal response classes (early, medium, late and pause). (**e**) Corollary discharge responses of putative mossy fibers recorded extracellularly in the EGp. Each row represents the smoothed and normalized average firing rate of a single mossy fiber, with ten examples of each class shown. (**f**) Corollary discharge responses of UBCs ($n = 19$ responses) and Golgi cells ($n = 8$ responses) recorded intracellularly. Each row represents the smoothed and normalized average firing rate of a single cell. Note the similarity with late and pause mossy fibers, shown in **e**.

granule cells[13,14]. Whole-cell recordings from UBCs provided direct support for this idea. We could clearly distinguish UBCs, granule cells and Golgi cells ($n = 54$, 184 and 11 recordings, respectively) on the basis of their electrophysiological properties and morphology (**Supplementary Figs. 1–3**). Corollary discharge responses in UBCs are delayed and diverse, and they closely resemble late and pause responses recorded extracellularly (**Fig. 1e**,**f**). An objective classification algorithm supported our conclusion that early and medium responses are extrinsic mossy fiber axons originating from midbrain nuclei but that late and pause responses are intrinsic mossy fiber axons originating from UBCs (**Supplementary Fig. 4**).

Our intracellular recordings revealed possible mechanisms for generating diverse and delayed responses in UBCs. We observed prominent post-inhibitory rebound firing in a subset of UBCs (**Fig. 2a** and **Supplementary Fig. 2**), so rebound evoked by an inhibitory input arriving at a short delay after the EOD command (**Fig. 2b** and **Supplementary Fig. 5a**) could account for delayed firing in UBCs. Suggestive of such a mechanism, the morphologically identified UBC shown in **Figure 2a**,**b** fired bursts at a long delay after the command that were stronger when the preceding membrane potential was more hyperpolarized. Other UBCs exhibited regular tonic firing (**Supplementary Fig. 2**) that, when terminated by hyperpolarization, was followed by precisely time-locked spikes (**Fig. 2c**). This firing pattern is similar to pause responses recorded extracellularly and could also be explained by inhibition arriving at a short delay after the command (**Fig. 2d** and **Supplementary Fig. 5a**). Golgi cells respond at short delays after the EOD command (**Fig. 1f** and **Supplementary Fig. 5b**) and could be the source of such inhibition.

Corollary discharge responses in granule cells

We next cataloged corollary discharge responses in a large number of granule cells using whole-cell recording (**Fig. 3**). We observed corollary discharge responses in 170 of 184 granule cells, and these responses consisted of prominent depolarizations with temporal patterns that were highly consistent across commands (**Fig. 3a**,**b** and **Supplementary Fig. 5c**,**d**). Granule cell depolarizations closely resembled early, medium, late, pause or, in some cases, apparent mixtures of these responses (**Fig. 3b** and **Supplementary Fig. 5d**). Action-potential firing consisted mainly of single spikes (1.25 spikes per command for the roughly 20% of granule cells that fired on greater than 10% of commands) and always occurred at the peak of the subthreshold membrane potential (**Fig. 4** and **Supplementary Fig. 6**).

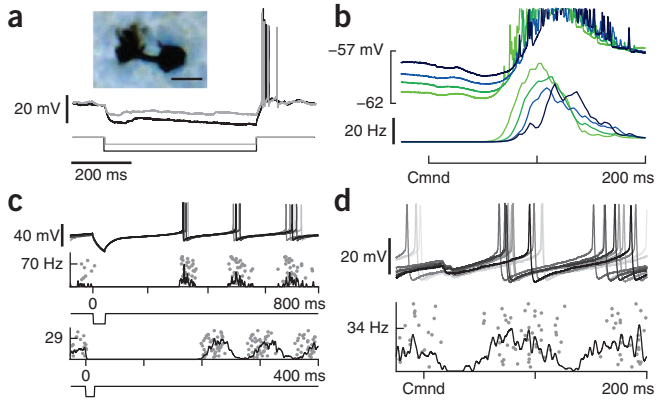

Figure 2 Mechanisms for delayed and diverse corollary discharge responses in UBCs. (**a**) Two overlaid traces illustrating prominent rebound firing in response to hyperpolarizing current injections (–10 pA and –20 pA) in a UBC. This cell was filled with biocytin allowing for *post hoc* morphological identification (inset; scale bar, 10 μm). Rebound firing was observed in 30 of 54 recorded UBCs. (**b**) Late corollary discharge response in the same UBC recording shown in **a**. In this cell the strength of late action potentials bursts (bottom traces) is related to the extent of preceding membrane potential hyperpolarization (top traces), suggesting rebound from command-locked hyperpolarization as a possible mechanism underlying late responses observed in UBCs. (**c**) Two UBCs in which a brief hyperpolarizing current injection (–50 pA, top; –200 pA, bottom) resulted in an entrainment of tonic firing, similar to temporal patterns of action potential firing observed in pause mossy fibers. Data are representative of 9 UBCs. (**d**) Pause-type corollary discharge response in a UBC. This cell exhibited a small hyperpolarization time-locked to the command and an entrainment of tonic action potential firing after the pause.

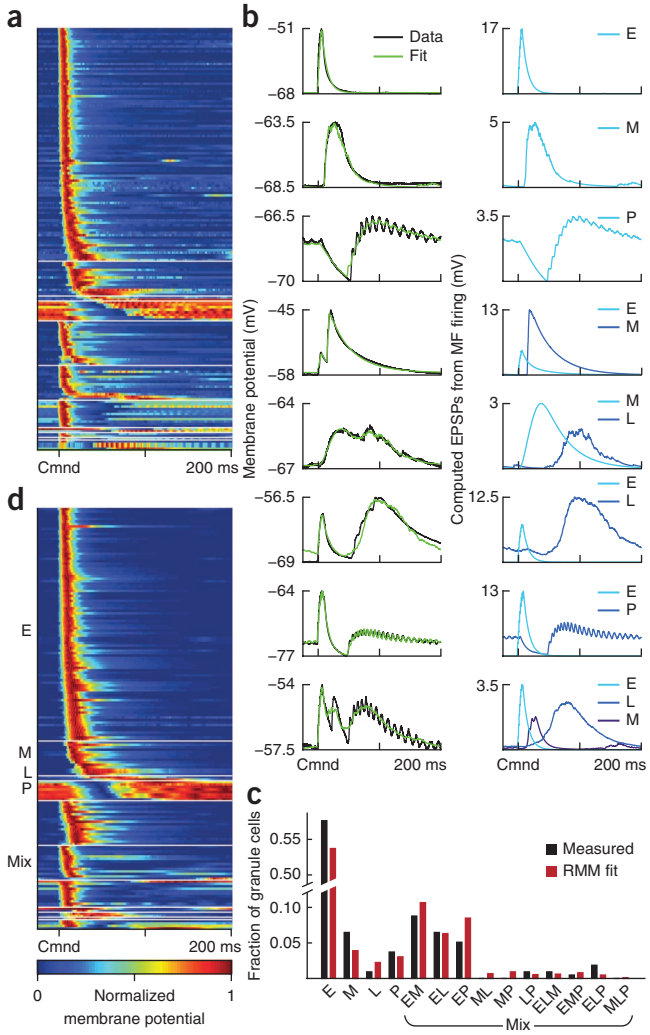

Figure 3 Experimental characterization and modeling of corollary discharge responses in granule cells. (**a**) Average subthreshold corollary discharge responses of 170 granule cells. Responses were grouped by category (see **d**) and then sorted by the latency of their peak membrane potential. (**b**) Left, examples of recorded granule cell subthreshold responses (data) and model fits (fit). Right, EPSPs computed from the recorded mossy fiber inputs used to fit each granule cell, labeled according to the class to which they belong. E, early; M, medium; L, late; P, pause. (**c**) Distribution of response categories assigned to recorded granule cells based on model fits (measured). Bars labeled E, M, L and P indicate the fraction of early, medium, late and pause inputs used to fit the recorded granule cell responses. Bars labeled "mix" show these fractions for combinations of inputs used in the same way. These fractions are consistent with a four-parameter random mixing model (RMM; parameters are the probability of early, medium, late and pause inputs) in which each input to a granule cell is assigned independently of the others (RMM fit). This suggests that the combinations of inputs granule cells receive are random. (**d**) Average subthreshold corollary discharge responses of 170 randomly constructed model granule cells selected from a total of 20,000. In this sample, the number of model cells from each granule cell category was matched to the experimental data, but the selection process was otherwise random. Note that the temporal response properties of the model granule cells closely resemble those of the recorded granule cell shown in **a**.

These observations led us to hypothesize that the temporal structure of subthreshold granule cell corollary discharge responses is shaped primarily by summation of excitatory inputs, rather than by phasic Golgi cell inhibition or the intrinsic properties of the granule cells themselves. To test this, we modeled granule cell depolarizations as sums of excitatory postsynaptic potentials (EPSPs) computed from the spike trains of up to three of the recorded EGp mossy fibers (**Fig. 1e**), including UBCs (**Fig. 1f**). The small number of excitatory inputs is consistent with anatomical observations that mormyrid granule cells have, on average, three claw-like dendritic endings (N.S., unpublished observations) and previous physiological observations indicating that granule cells receive other sources of mossy fiber input in addition to corollary discharge, for example, proprioceptive input from spinocerebellar mossy fibers[15]. By choosing an appropriate set of inputs from the recorded data and adjusting their excitatory synaptic strengths within a reasonable range (**Fig. 3b** and Online Methods), we were able to fit the membrane-potential responses of the recorded granule cells with high accuracy (average mean squared error = 4.6%, $n = 169$ recordings; **Fig. 3b** and **Supplementary Fig. 6**). This provides strong support for the view of granule cell recoding as a summation of excitatory inputs stated above.

The similarity of the constructed and recorded granule cell responses also provides a powerful tool for addressing the central question of whether granule cell responses can support negative-image formation and sensory cancellation. Given the sparseness of granule cell firing that we observed (both a small percentage of granule cells that fired and a small number of spikes per EOD in those that did), cancellation likely depends on large numbers of granule cell inputs; indeed, anatomical estimates are on the order of 20,000 granule cell inputs per medium ganglion cell[16]. To expand the data to this number, we constructed model granule cells. This was aided by the fact that the distribution of inputs found in our fits of recorded granule cell responses is consistent with a random mixing process in which each granule cell dendrite samples the different functional input classes (early, medium, late and pause) independently (**Fig. 3c**). We extracted the probability of a granule cell receiving an input from each functional class from these fits (Online Methods). Drawing randomly from these input probabilities and from the distribution of synaptic weights obtained during fitting allowed us to construct model granule cells with corollary discharge responses that closely match those of the recorded granule cells (**Fig. 3d** and **Supplementary Fig. 6**; note that these are not granule cells fit to the data, but randomly constructed and sampled model cells). The remarkable similarity between these model responses and the data provides additional support for the hypothesis that granule cell recoding of corollary discharge inputs can be explained by random mixtures of small numbers of excitatory inputs conveyed by extrinsic mossy fibers and UBCs.

Spiking in model granule cells was implemented by randomly assigning action potential thresholds sampled from a normal distribution fit to the thresholds of the recorded granule cells (average distance to threshold 20.2 ± 5.97 mV (± s.d.)). The resulting temporal firing patterns and distribution of average spike counts per EOD in the model granule cells were statistically consistent with those of the recorded granule cells (**Fig. 4** and **Supplementary Fig. 6**).

Granule cells provide a basis for sensory cancellation

Previous experimental work has revealed a combination of anti-Hebbian spike timing–dependent long-term synaptic depression and non-associative long-term potentiation at granule cell–medium ganglion cell synapses[5,17]. To determine whether this form of plasticity can cancel self-generated sensory input using realistic granule cell responses, we drove a passive model medium ganglion cell with 20,000 model granule cell inputs through plastic synapses. The granule cell–medium ganglion cell synapses were strictly positive, and we

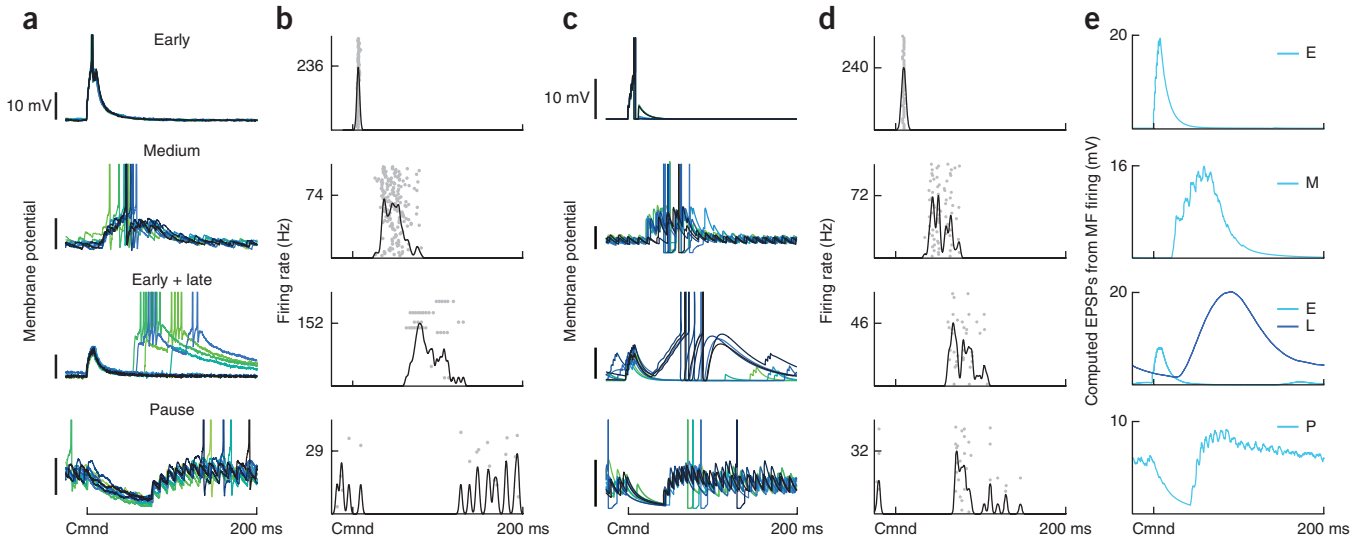

Figure 4 Patterns of corollary discharge-evoked action-potential firing in recorded and model granule cells. (**a**) Corollary discharge responses of four recorded granule cells that spiked in response to the EOD command. Granule cell membrane potentials from several commands are overlaid. Spikes were truncated to show details of subthreshold membrane potentials. (**b**) Spiking responses of the recorded granule cells shown in **a**. Spike trains on 50 individual trials are shown in gray, and the smoothed (5 ms Gaussian kernel) trial-averaged firing rate of the cell is overlaid in black. (**c**,**d**) Corollary discharge responses of four model granule cells selected from among the pool of 20,000 generated cells. Displays for model granule cells are the same as for recorded cells. (**e**) Sources of mossy fiber input to each model granule cell, as computed EPSPs from the trial-averaged mossy fiber firing rates. Both subthreshold corollary discharge responses and spiking in model granule cells closely resembles that seen in recorded granule cells.

initially set their strengths so that granule cell responses in the absence of EOD-driven sensory input generated a roughly flat medium ganglion membrane potential, consistent with recordings from medium ganglion cells in regions of the ELL involved in passive electrosensory processing[2,6,7]. Next, we added a temporally varying sensory input to the model medium ganglion cell to mimic the responses of passive electroreceptors to the fish's own EOD recorded in a previous study[1] (**Fig. 5a**). As in previous modeling work[3], the strength of the granule cell–medium ganglion synapses evolved according to the experimentally described plasticity rule[5,17]: synaptic strength was increased for each presynaptic action potential, corresponding to experimentally described non-associative potentiation, and decreased when a postsynaptic action potential occurred shortly after a presynaptic action potential, corresponding to experimentally described associative depression. Over the course of about 1,000 EOD commands (~5 min at EOD command rates typical of paralyzed fish), the membrane potential fluctuation caused by the sensory input was cancelled by the corollary discharge inputs conveyed by granule cells (**Fig. 5a**), consistent with the timecourse over which negative images are formed *in vivo*[2,6]. The resulting negative image closely matched the inverse of the sensory input (**Fig. 5b**) and had small command-to-command variations (**Fig. 5b**; s.d. of ~1 mV) despite the sparseness of the

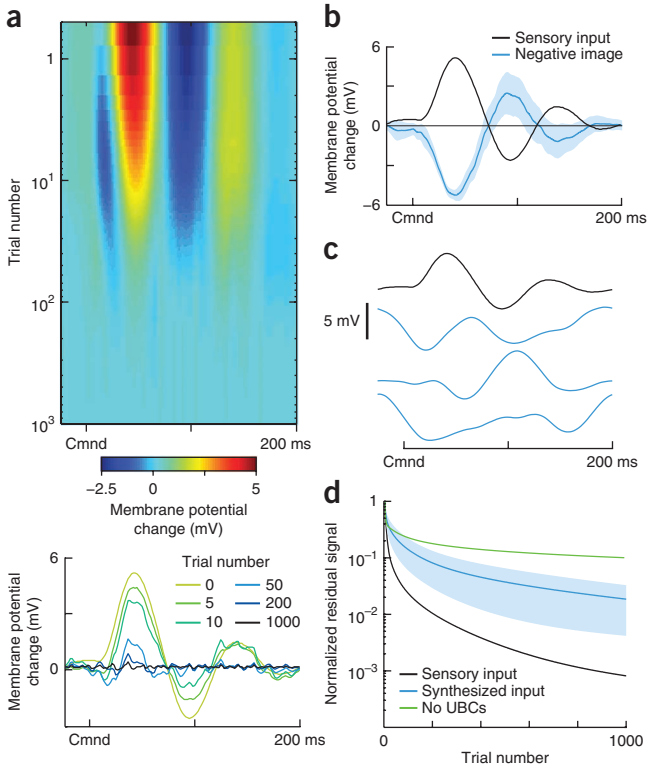

Figure 5 Granule cell corollary discharge responses provide an effective basis for cancelling natural patterns of self-generated sensory input. (**a**) Top, cancellation of the change in membrane potential caused by sensory input locked to the EOD motor command in a model medium ganglion cell. The medium ganglion cell received 20,000 model granule cell inputs with synaptic strengths that were adjusted by anti-Hebbian spike timing–dependent plasticity. Bottom, select trials showing the time course of cancellation. The temporal profile of the sensory input (trial 0) was chosen to resemble the effects of the EOD on passive electroreceptors recorded in a previous study[1]. (**b**) The effect of the sensory input on medium ganglion cell membrane potential (sensory input) and the negative image (shaded region shows ±1 s.d. across trials). (**c**) Different input signals used for the tests of sensory cancellation rates shown in **d**. The top trace is the same input used in **a**, and resembles natural self-generated inputs owing to the EOD. The blue traces were selected from a set of 1,000 synthesized inputs with the same power spectrum as the natural input but with randomized phases. (**d**) Comparison of the time course of cancellation for the natural sensory input versus the synthesized inputs (shaded region is ±1 s.d.). Note that cancellation was faster for the natural input, suggesting that the structure of granule cell responses is matched to the temporal pattern of the self-generated signal. Cancellation was also much slower and less effective if the model granule cells were generated without UBC inputs (no UBCs).

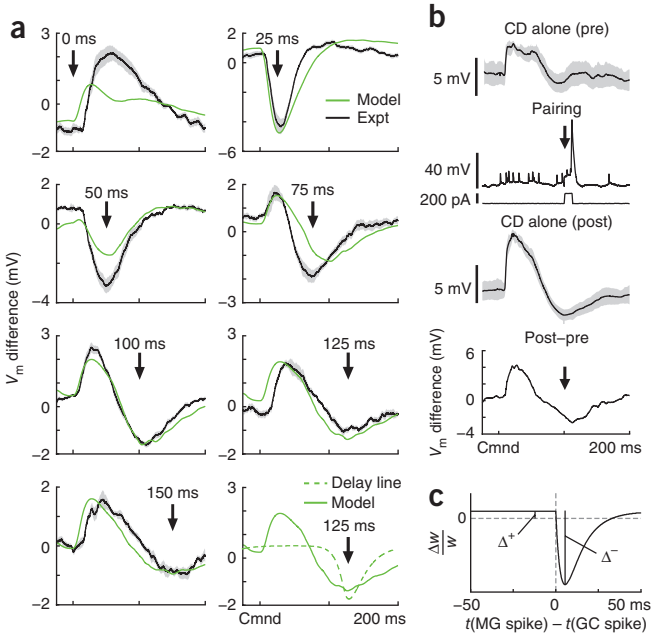

Figure 6 Non-uniform temporal structure of granule cell responses predicts specific features of negative images in medium ganglion cells. (**a**) Changes in corollary discharge responses induced by pairing with medium ganglion dendritic spikes at seven different delays after the EOD command. Green traces are membrane potential (V_m) differences derived from the model with fitted values for the magnitudes of associative depression and non-associative potentiation (**c**). Black traces are experimentally observed membrane potential differences averaged across medium ganglion cells (shaded regions represent s.e.m.; 0 ms, $n = 6$ cells; 25 ms, $n = 8$; 50 ms, $n = 6$; 75 ms, $n = 6$; 100 ms, $n = 10$; 125 ms, $n = 4$; 150 ms, $n = 3$). The bottom right graph compares these predictions with those for a delay line basis (dashed green line). (**b**) Design of the pairing experiment. Intracellular traces from an medium ganglion cell showing the average (black) and s.d. (gray outline) of the corollary discharge (CD) response before (pre), during (pairing) and after (post) 3 min of pairing during which a brief (12 ms) intracellular current injection evoked a dendritic spike at a fixed delay after the EOD command (arrow). The small spikes are axonal spikes and do not contribute to plasticity[5]. The bottom trace (post-pre) shows the difference in the membrane potential induced by the pairing, corresponding to the traces shown in **a**. Note the complex pattern of change: a relative hyperpolarization around the time of the paired spike as well as a large relative depolarization just after the command, as predicted by the model. (**c**) Synaptic plasticity rule and parameters used for the fits shown in **a**. Δ^+ is the magnitude of the non-associative potentiation and Δ^- is the magnitude of the associative depression.

granule cell firing. We also confirmed the stability of negative images formed using the granule cells as a temporal basis (**Supplementary Modeling**) and that the changes in synaptic strength underlying negative images were within a physiologically plausible range (**Supplementary Fig. 7**). Finally, because our estimates of both the number of granule cells active at long delays and the number of command-locked action potentials fired by granule cells were based on limited data, we tested the effects of systematically varying these properties of the model granule cells on negative images and sensory cancellation (**Supplementary Figs. 8** and **9**). We observed rapid cancellation and negative images with small command-to-command variations even when we reduced the numbers of late and pause inputs used to generate model granule cells, and when we reduced the number of command-locked action potentials fired by granule cells.

The effectiveness of the cancellation in the model is notable given the highly non-uniform temporal structure of the response of the granule cell population, in particular the fact that most granule cells are active at short delays. Rather than a general-purpose temporal basis, such as the delay-line model considered in previous theoretical work[3], the structure of granule cell corollary discharge responses appears to be matched to the temporal patterns of self-generated sensory input that the fish encounters in nature, i.e., the particular pattern of ringing that the large EOD evokes in electroreceptors tuned to detect much smaller signals[1]. To test this idea more directly, we generated synthetic inputs with different temporal profiles but the same power spectrum as the electroreceptor response (**Fig. 5c**). Synthetic inputs were cancelled more slowly than inputs resembling the electroreceptor response (**Fig. 5d**), suggesting that the structure of granule cell responses is particularly suited to natural patterns of self-generated input. Furthermore, the rate and accuracy of sensory cancellation in the granule cell basis is comparable to that of an idealized uniform delay line basis with tuning widths approximately equal to that of granule cells receiving medium and late inputs (**Supplementary Fig. 10**). Finally, we note that model granule cell populations lacking late and pause inputs provided a far less effective basis for cancellation (**Fig. 5d**), indicating an important role for the temporally diverse and delayed corollary discharge responses generated by UBCs.

Granule cell responses predict features of negative images

Our knowledge of the temporal structure of granule cell responses allowed us to make specific predictions about the shapes of negative images induced in experiments in which a single dendritic spike in a medium ganglion cell is paired with the EOD command at fixed delays. Previous studies have shown that such dendritic spikes are the key triggers for associative depression at granule cell synapses[5,18]. Our predictions based on the measured granule cell responses were twofold (**Fig. 6a**). Medium ganglion cell spikes evoked at short delays should induce a brief hyperpolarization peaked around the spike time due to associative depression of early granule cells inputs. We predicted more complex, biphasic changes for medium ganglion cell spikes evoked either at longer delays or at zero delay. At such delays, associative depression should induce a hyperpolarization around the medium ganglion cell spike time, whereas non-associative potentiation of the numerous early granule cell inputs should cause a 'paradoxical' medium ganglion cell depolarization at short delays after the EOD command. In contrast, a model with a temporally uniform delay line basis predicted that negative images induced by medium ganglion cell spikes at different delays would always have the same shape, determined by the temporal window of the synaptic plasticity, and differ only by time translation (**Fig. 6a**).

To test these model predictions, we recorded intracellularly from medium ganglion cells, and compared corollary discharge responses before and after 3 min of pairing (~600 commands) with a brief injection of current that evoked a dendritic spike at a fixed delay after the EOD command (**Fig. 6b**). The shapes of the resulting negative images exhibited a strong dependence on the delay during pairing, in agreement with our qualitative predictions (**Fig. 6a**). Furthermore, close quantitative agreement between our model and the experimental medium ganglion cell response changes (**Fig. 6a**) could be achieved by fitting just two parameters of the synaptic plasticity rule (**Fig. 6c** and Online Methods). The similarity of the modeled and measured changes in medium ganglion cell responses indicates that the measured granule cell responses and previously measured anti-Hebbian plasticity at granule cell-medium ganglion cell synapses accurately describe formation of negative images.

DISCUSSION

Using intracellular recordings and modeling of granule cells in mormyrid fish, we provided a relatively complete description of granule cell recoding, far more complete than that available in other systems. The remarkably close agreement between recorded and model granule cells (**Fig. 3**) strongly suggests that the simple rules we used to transform mossy fiber inputs into granule cell responses, i.e., summation of randomly selected excitatory inputs, are essentially correct and complete. Such a complete understanding of how inputs are transformed into output *in vivo* is remarkable in its own right and places us in a unique position to explore the relationships between input coding, an experimentally defined synaptic plasticity rule[5,17] and a well-characterized adaptive network output in the form of negative images[2,6,7]. Though input coding and plasticity are the critical elements for the functioning of many neural circuits, including other cerebellum-like circuits[19–21] and the cerebellum itself[22–25], there are few cases in which these elements are understood so thoroughly.

The function of EGp circuitry demonstrated here closely parallels longstanding, but still untested, expansion-recoding schemes posited for the granular layer of the mammalian cerebellum[22,23]. Whereas most models of the function of the cerebellar granular layer posit pivotal roles for Golgi cell inhibition of granule cells in expansion recoding[24], our study suggests a key role for UBCs. Though we had no way to specifically target UBCs and hence cannot provide a complete account of their properties, our *in vivo* intracellular recordings suggest that they generate temporally diverse and delayed responses that are faithfully recoded in granule cells. Though *in vivo* responses to discrete inputs have yet to be described for UBCs in the mammalian cerebellum or dorsal cochlear nucleus, *in vitro* studies have documented a variety of synaptic and intrinsic mechanisms that can generate prolonged and/or delayed responses[26–30]. These include rebound firing[29], regular tonic firing[29] and inhibitory synaptic input from Golgi cells[30], the key ingredients for delayed responses suggested by our *in vivo* intracellular recordings. Hence the functions for UBCs established here may extend to other circuits in which they are found. Finally, though the capacity to generate temporally diverse responses in granule cells may be useful for a variety of cerebellar computations, the density of UBCs varies widely across different regions of the cerebellum and across different species[31]. Whether other circuit mechanisms, e.g., phasic Golgi cell inhibition of granule cells, function to generate temporally diverse granule cell responses for regions of the cerebellum in which UBCs are scarce is an important question for future studies.

An unexpected finding of this study is that rather than a general temporal basis, such as delay-line models considered in previous theoretical work[3], the temporal structure of granule cell responses is highly non-uniform. Despite the fact that the preponderance of granule cells are active at short delays, our modeling suggests that granule cells provide a highly effective basis for sensory cancellation. The explanation for this apparent paradox is that the temporal structure of granule cell responses, though not necessarily optimal or superior to a delay-line basis, is well-suited to cancel natural patterns of self-generated sensory input. How such apparent matching might occur and whether it could be modified by experience are interesting questions for future investigations. The non-uniform temporal structure of granule cell responses also provides a simple explanation for unusual features of medium ganglion cell negative images formed in response to artificial inputs. The ability to accurately predict detailed features of negative images based on modeled granule cell responses, and previously described anti-Hebbian plasticity, also provides an additional experimental validation for the links we established between input coding, plasticity and adaptive network output. Finally, the apparent matching between granule cell responses and natural patterns of self-generated sensory input does not imply that the system cannot provide effective cancellation when conditions change. Indeed, EOD amplitude along with passive electroreceptor responses to the EOD are expected to change on multiple timescales due to growth of the fish, seasonal changes in water conductivity and the presence of large nonconducting objects near the fish. However, as has been shown in a previous study of the effects of water conductivity on passive electroreceptor responses[1], such changes will primarily affect the size rather than the temporal structure of sensory responses to the EOD. Hence the matching between the temporal structure of granule cell responses and self-generated sensory input described here is expected to hold over a wide range of behaviorally relevant conditions.

Though the notion that motor corollary discharge signals could be used to predict and cancel the sensory consequences of an animal's own behavior has a long history[32,33], there are few cases in which such functions have been characterized at the level of neural circuits[34]. In particular, it has proven challenging to understand how copies of motor commands are translated into an appropriate format to cancel sensory inputs. This problem takes a particularly clear and tractable form in the case of mormyrid ELL, where copies of a brief, highly stereotyped motor command must be delayed and diversified in order to provide a basis for cancelling sensory effects that are extended in time. A major contribution of our study is that we directly demonstrated that such a temporal expansion indeed occurs in granule cells and that, along with previously described anti-Hebbian plasticity[5,17], this expansion is sufficient to account for negative images. Our results thus provide the critical missing piece in a relatively complete mechanistic account of how motor commands are used to predict sensory consequences at the levels of synaptic plasticity, cells and circuits.

METHODS

Methods and any associated references are available in the online version of the paper.

Note: Any Supplementary Information and Source Data files are available in the online version of the paper.

ACKNOWLEDGMENTS

This work was supported by grants from the US National Science Foundation (1025849), US National Institutes of Health (NIH; NS075023), Alfred P. Sloan Foundation and the McKnight Endowment Fund for Neuroscience to N.B.S.; NIH grant (MH093338) to L.F.A.; and a Howard Hughes Medical Institute International Student Research Fellowship to P.K.; A.K. was supported by NIH training grant T32NS064929. Additional support was provided by the Gatsby Foundation, the Swartz Foundation and the Kavli Institute for Brain Science at Columbia University. We thank R. Axel and T. Jessell for comments on the manuscript, and K. Zhang for assistance with histology.

AUTHOR CONTRIBUTIONS

N.B.S. and K.A. performed the experiments. A.K., G.W. and P.K. performed the modeling. N.B.S., L.F.A., A.K., G.W. and P.K. wrote the manuscript. N.B.S. and L.F.A. designed and supervised the project.

COMPETING FINANCIAL INTERESTS

The authors declare no competing financial interests.

1. Bell, C.C. & Russell, C.J. Effect of electric organ discharge on ampullary receptors in a mormyrid. *Brain Res.* **145**, 85–96 (1978).
2. Bell, C.C. An efference copy modified by reafferent input. *Science* **214**, 450–453 (1981).
3. Roberts, P.D. & Bell, C.C. Computational consequences of temporally asymmetric learning rules: II. sensory image cancellation. *J. Comput. Neurosci.* **9**, 67–83 (2000).

4. Williams, A., Roberts, P.D. & Leen, T.K. Stability of negative-image equilibria in spike-timing-dependent plasticity. *Phys. Rev. E* **68**, 021923 (2003).
5. Bell, C.C., Han, V.Z., Sugawara, S. & Grant, K. Synaptic plasticity in a cerebellum-like structure depends on temporal order. *Nature* **387**, 278–281 (1997).
6. Bell, C.C. Properties of a modifiable efference copy in electric fish. *J. Neurophysiol.* **47**, 1043–1056 (1982).
7. Bell, C.C., Caputi, A., Grant, K. & Serrier, J. Storage of a sensory pattern by anti-Hebbian synaptic plasticity in an electric fish. *Proc. Natl. Acad. Sci. USA* **90**, 4650–4654 (1993).
8. Bell, C.C., Grant, K. & Serrier, J. Corollary discharge effects and sensory processing in the mormyrid electrosensory lobe: I. Field potentials and cellular activity in associated structures. *J. Neurophysiol.* **68**, 843–858 (1992).
9. Bell, C. & von der Emde, G. Electric organ corollary discharge pathways in mormyrid fish: II. The medial juxtalobar nucleus. *J. Comp. Physiol. A Neuroethol. Sens. Neural Behav. Physiol.* **177**, 463–479 (1995).
10. Sawtell, N.B., Mohr, C. & Bell, C.C. Recurrent feedback in the mormyrid electrosensory system: cells of the preeminential and lateral toral nuclei. *J. Neurophysiol.* **93**, 2090–2103 (2005).
11. von der Emde, G. & Bell, C. Nucleus preeminentialis of mormyrid fish, a center for recurrent electrosensory feedback. I. electrosensory and corollary discharge responses. *J. Neurophysiol.* **76**, 1581–1596 (1996).
12. Mugnaini, E., Sekerkova, G. & Martina, M. The unipolar brush cell: A remarkable neuron finally receiving deserved attention. *Brain Res. Rev.* **66**, 220–245 (2011).
13. Campbell, H.R., Meek, J., Zhang, J. & Bell, C.C. Anatomy of the posterior caudal lobe of the cerebellum and the eminentia granularis posterior in a mormyrid fish. *J. Comp. Neurol.* **502**, 714–735 (2007).
14. Meek, J., Yang, J.Y., Han, V.Z. & Bell, C.C. Morphological analysis of the mormyrid cerebellum using immunohistochemistry, with emphasis on the unusual neuronal organization of the valvula. *J. Comp. Neurol.* **510**, 396–421 (2008).
15. Sawtell, N.B. Multimodal integration in granule cells as a basis for associative plasticity and sensory prediction in a cerebellum-like circuit. *Neuron* **66**, 573–584 (2010).
16. Meek, J. *et al.* Interneurons of the ganglionic layer in the mormyrid electrosensory lateral line lobe: morphology, immunocytochemistry, and synaptology. *J. Comp. Neurol.* **375**, 43–65 (1996).
17. Han, V.Z., Grant, G. & Bell, C.C. Reversible associative depression and nonassociative potentiation at a parallel fiber synapse. *Neuron* **27**, 611–622 (2000).
18. Engelmann, J. *et al.* Dendritic backpropagation and synaptic plasticity in the mormyrid electrosensory lobe. *J. Physiol. Paris* **102**, 233–245 (2008).
19. Bell, C.C., Han, V. & Sawtell, N.B. Cerebellum-like structures and their implications for cerebellar function. *Annu. Rev. Neurosci.* **31**, 1–24 (2008).
20. Farris, S.M. Are mushroom bodies cerebellum-like structures? *Arthropod Struct. Dev.* **40**, 368–379 (2011).
21. Oertel, D. & Young, E.D. What's a cerebellar circuit doing in the auditory system? *Trends Neurosci.* **27**, 104–110 (2004).
22. Albus, J.S. A theory of cerebellar function. *Math. Biosci.* **10**, 25–61 (1971).
23. Marr, D. A theory of cerebellar cortex. *J. Physiol. (Lond.)* **202**, 437–470 (1969).
24. Medina, J.F. & Mauk, M.D. Computer simulation of cerebellar information processing. *Nat. Neurosci.* **3**, 1205–1211 (2000).
25. Dean, P., Porrill, J., Ekerot, C.F. & Jorntell, H. The cerebellar microcircuit as an adaptive filter: experimental and computational evidence. *Nat. Rev. Neurosci.* **11**, 30–43 (2010).
26. Diana, M.A. *et al.* T-type and L-type Ca^{2+} conductances define and encode the bimodal firing pattern of vestibulocerebellar unipolar brush cells. *J. Neurosci.* **27**, 3823–3838 (2007).
27. Locatelli, F., Botta, L., Prestori, F., Masetto, S. & D'Angelo, E. Late-onset bursts evoked by mossy fibre bundle stimulation in unipolar brush cells: evidence for the involvement of H- and TRP-currents. *J. Physiol.* **591**, 899–918 (2013).
28. Rossi, D.J., Alford, S., Mugnaini, E. & Slater, N.T. Properties of transmission at a giant glutamatergic synapse in cerebellum: the mossy fiber-unipolar brush cell synapse. *J. Neurophysiol.* **74**, 24–42 (1995).
29. Russo, M.J., Mugnaini, E. & Martina, M. Intrinsic properties and mechanisms of spontaneous firing in mouse cerebellar unipolar brush cells. *J. Physiol.* **581**, 709–724 (2007).
30. Rousseau, C.V. *et al.* Mixed inhibitory synaptic balance correlates with glutamatergic synaptic phenotype in cerebellar unipolar brush cells. *J. Neurosci.* **32**, 4632–4644 (2012).
31. Mugnaini, E., Sekerková, G. & Martina, M. The unipolar brush cell: a remarkable neuron finally receiving deserved attention. *Brain Res. Rev.* **66**, 220–245 (2011).
32. Sperry, R.W. Neural basis of the spontaneous optokinetic response produced by visual inversion. *J. Comp. Physiol. Psychol.* **43**, 482–489 (1950).
33. von Holst, E. & Mittelstaedt, H. The reafference principle. *Naturwissenschaften* **37**, 464–476 (1950).
34. Crapse, T.B. & Sommer, M.A. Corollary discharge across the animal kingdom. *Nat. Rev. Neurosci.* **9**, 587–600 (2008).

ONLINE METHODS

Experimental preparation. All experiments performed in this study adhere to the American Physiological Society's Guiding Principles in the Care and Use of Animals and were approved by the Columbia University Institutional Animal Care and Use Committee. Mormyrid fish (7–12 cm in length) of the species *Gnathonemus petersii* were used in these experiments. Surgical procedures to expose EGp for recording were identical to those described previously[15]. Gallamine triethiodide (Flaxedil) was given at the end of the surgery (~20 μg/cm of body length) and the anesthetic (MS:222, 1:25,000) was removed. Aerated water was passed over the fish's gills for respiration. Paralysis blocks the effect of electromotoneurons on the electric organ, preventing the EOD, but the motor command signal that would normally elicit an EOD continues to be emitted by the electromotoneurons at a variable rate of 2 to 5 Hz. The timing of the EOD motor command can be measured precisely (see below) and the central effects of corollary discharge inputs can be observed in isolation from the electrosensory input that would normally result from the EOD.

Electrophysiology. The EOD motor command signal was recorded with an electrode placed placed over the electric organ. The command signal is the synchronized volley of electromotoneurons that would normally elicit an EOD in the absence of neuromuscular blockade. The command signal lasts about 3 ms and consists of a small negative wave followed by three larger biphasic waves. The latencies of central corollary discharge or command-evoked responses were measured with respect to the negative peak of the first large biphasic wave in the command signal. Extracellular recordings from mossy fibers in EGp were made using glass microelectrodes filled with 2 M NaCl (40–100 MΩ), as described previously[8,15]. For *in vivo* whole-cell recordings from EGp neurons and from medium ganglion cells in ELL electrodes (9–15 MΩ) were filled with an internal solution containing (in mM) K-gluconate (122), KCl (7), HEPES (10), Na_2GTP (0.4), MgATP (4), EGTA (0.5) and 0.5% biocytin (pH 7.2, 280–290 mOsm). No correction was made for liquid-junction potentials. Only cells with stable membrane potentials more hyperpolarized than −50 mV and access resistance <100 MΩ were analyzed. Membrane potentials were filtered at 3–10 kHz and digitized at 20 kHz (CED power1401 hardware and Spike2 software; Cambridge Electronics Design).

Extracellular mossy fiber recordings. Several independent lines of evidence suggest that early, medium, late and pause responses obtained using extracellular recordings in EGp (**Fig. 1d,e**) reflect the activity of mossy fiber axons (either extrinsic mossy fibers originating from sources outside of EGp or intrinsic mossy fibers arising from UBCs), rather than granule cells or Golgi cells. (i) Recordings attributed to mossy fibers had characteristics similar to those made previously from known fiber tracts, including tracts containing mossy fiber axons destined for EGp. These include very large, mainly positive spike waveforms[8,15], as well as sudden and often brief isolation. (ii) Firing properties of putative mossy fiber recordings closely matched those of units recorded in mossy fiber nuclei of origin in the midbrain and those of UBCs, but differed markedly from those of granule cells, in which action potential firing was much sparser. (iii) Characteristic early, medium, late and pause responses of putative extracellular mossy fiber recordings were also observed in a much smaller number of whole-cell recordings from mossy fiber axons. The latter can be identified, unambiguously, based on distinctive electrophysiological properties similar to those reported for mossy fiber bouton recordings in the mammalian cerebellum[35], including: spikes with prominent afterdepolarizations, lack of repetitive firing in response to sustained depolarizing current injections, and complete lack of synaptic activity.

Objective classification of mossy fibers. To classify mossy fibers, we fit a multinomial logistic regression model to features of the corollary discharge responses of cells recorded in PCA ($n = 12$ recordings), PE ($n = 28$) and UBCs ($n = 10$), and used this model to assign labels of early, medium or late to the recorded mossy fibers. We selected three response features that gave low classifier error on a validation set (fivefold cross validation error: 2.67%). (i) Time of first rise: the first time relative to the EOD at which the smoothed (Gaussian kernel, $\tau = 5$ ms), trial-averaged firing rate achieves 75% of its maximum. (ii) Half-width of response: the width of the first peak for which the smoothed, trial-averaged firing rate is above 50% of its maximum rate. (iii) Spiking variability: the variance of the cell's spike times relative to the EOD, given by $(1/N)\Sigma_{i=1}^{N}(t_i - t)^2$, where t_i is the time of the ith recorded spike relative to the most recent EOD command and $t = (1/N)\Sigma_{i=1}^{N} t_i$.

Dendritic spike pairing experiments. Methods for dendritic spike pairing experiments in medium ganglion cells were similar to those described previously[15]. Effects of pairing on corollary discharge responses were evaluated based on averages of 60 s (responses to approximately 200 EOD motor commands) of data taken immediately before and after the pairing period. In some cases, narrow spikes were removed using a median filter before averaging. Dendritic spikes were induced by brief (12–15 ms) intracellular current injections (100–600 pA). The duration of the pairing period was 3 min. Baseline rate of broad spike firing were extremely low such that during pairing, few if any spontaneous broad spikes occurred. Cells in which resting membrane potential, access resistance, or spike height changed substantially over the course of the experiment were excluded from the analysis. Consistent with previous results, plastic changes decayed gradually over the course of approximately 3–5 min after the end pairing. Because medium ganglion cell recordings were difficult to obtain, but often extremely stable, multiple pairings at different delays were conducted in some cells after allowing effects of the previous pairing to decay.

Histology. After recording, fish were deeply anesthetized with a concentrated solution of MS:222 (1:10,000) and perfused through the heart with a teleost Ringer solution followed by a fixative, consisting of 2% (wt/vol) paraformaldehyde and 2% glutaraldehyde or 4% (wt/vol) paraformaldehyde in 0.1 M phosphate buffer. The brains were postfixed, cryoprotected with 20% sucrose and sectioned at 50 μM on a cryostat. Sections were reacted with avidin-biotin complex and diamino-benzidine or a streptavidin-conjugated fluorescent dye to reveal the biocytin filled cells.

Data analysis and statistics. Data were analyzed off-line using Spike2 and Matlab (MathWorks). Data are expressed as means ± s.d., unless otherwise noted. Paired and unpaired Student's t-tests were used to test for statistical significance, as noted. Differences were judged to be significant at $P < 0.05$.

Fitting measured granule cell responses. We modeled the granule cell as a passive unit with leak potential E_L, which received excitatory input from 1–3 mossy fibers (including UBCs) with firing rates $r^i(t)$. The membrane potential $V(t)$ of the model granule cell is determined by its mossy fiber inputs, filtered by the mossy fiber-granule cell EPSP $\mathcal{E}$, where $\mathcal{E}$ is the convolution of synaptic and membrane filters. The synaptic filter was modeled as a weighted sum of a fast and slow exponential filter, giving the model

$$V(t) = E_L + \sum_{i=1}^{N} w^i_{\text{fast}}(\mathcal{E}_{\text{fast}} * r^i)(t) + w^i_{\text{slow}}(\mathcal{E}_{\text{slow}} * r^i)(t)$$

The time constants of the synaptic filters were fit by hand to give $\tau_{\text{fast}} = 0.2$ ms and $\tau_{\text{slow}} = 37.8$ ms. The membrane time constant of the recorded granule cells was determined experimentally to be $\tau_m = 8.7$ ms.

To fit the responses of the recorded granule cells, we first found a set of candidate mossy fiber inputs by finding w^i_{fast} and w^i_{slow} that minimize

$$C(w^i_{\text{fast/slow}}) = \frac{1}{2T}\sum_{t=0}^{T}(\tilde{V}(t) - V(t))^2 + \alpha_1(||\mathbf{w}_{\text{slow}}||_1 + ||\mathbf{w}_{\text{fast}}||_1)$$

where T is the length of the command cycle, and $\tilde{V}(t)$ is the voltage of the model granule cell. We chose the smallest value of α_1 that produced 10 nonzero mossy fiber inputs. We constrained weights to be non-negative using an adjusted least-angle regression (LARS) solution of the LASSO problem[36] that selects only inputs which are positively correlated with the granule cell response. We next cut our candidates down to 1–3 mossy fibers by finding w^i_{fast} and w^i_{slow} that minimize

$$C(w^i_{\text{fast/slow}}) = \frac{1}{2T}\sum_{t=0}^{T}(\tilde{V}(t) - V(t))^2 + \alpha_0(||\mathbf{w}_{\text{slow}}||_0 + ||\mathbf{w}_{\text{fast}}||_0)$$

Here, we apply the L_0 norm to the weight vectors, which is the number of nonzero elements contained within them. Adjusting the value of α_0 gives the lowest mean squared error model fits that use one, two, or three mossy fiber inputs. For each

granule cell fit, we manually selected the value of α_0 that best captured all features of the recorded cell's average corollary discharge response. A subset of late mossy fibers fired action potentials on only a fraction of commands. We also observed prominent late subthreshold responses on only a fraction of commands in a subset of granule cells. For purposes of accurately fitting responses to such inputs, average mossy fiber spiking and average granule cell corollary discharge responses were computed using only those trials on which late spikes and synaptic responses were observed. For purposes of generating model granule cells, such non-spiking trials were included (see below).

Random mixing test. Granule cell categories (E, M, L, P, EM, EL, EP, ML, MP, LP, EML, EMP, ELP, MLP and N, where E is early, M is medium, L is late, P is pause and N is none) were assigned to the 169 recorded granule cells depending on the mossy fibers selected as inputs to the fit model granule cells. We constructed a random mixing model with the following assumptions. (i) Each granule cell has three sites for mossy fiber synaptic inputs. (ii) The probabilities of a given input being of E, M, L and P type are given by P_E, P_M, P_L and P_P, with $P_E + P_M + P_L + P_P \leq 1$. (iii) The type of input received at one mossy fiber-granule cell synapse is independent of that received at any other synapse. We fit the input type probabilities to the model granule cell fits by minimizing the chi-squared statistic. The category frequencies included all possible input combinations that produced a granule cell of a given category; for example, E_{EM} was calculated as

$$3P_E^2P_M + 3P_EP_M^2 + 6P_EP_M(1 - P_E - P_M - P_L - P_P)$$

Generating model cells. We introduced two sources of variability to our model based on observed sources of variability in recorded cells. We found trial-to-trial variability in peak height of recorded single EPSPs to be normally distributed with $\sigma = 0.224$ mV; during simulation of model granule cells, we sampled this distribution for each mossy fiber spike. As shown previously[15], in addition to receiving corollary discharge inputs, some granule cells (84 of 212 recorded in the present study) also receive input from mossy fibers that fire at high rates, independent of the EOD command. Many such 'tonic' mossy fibers convey proprioceptive information[8,15]. We added tonic input to our model based on 72 tonic mossy fibers recorded in a previous study[15]. The probability of a granule cell receiving tonic input was computed under the assumption of random mossy fiber mixing, and we set the synaptic weight of tonic inputs to model granule cells by sampling a Gaussian distribution fit to observed tonic EPSP sizes (2.5 ± 0.9 mV). Using the mossy fiber input probabilities fit from our random mixing model, we randomly determined whether each "dendrite" of a given model granule cell received early ($P_E = 0.425$), medium ($P_M = 0.075$), late ($P_L = 0.050$), pause ($P_P = 0.050$), tonic ($P_T = 0.157$) or no input ($P_N = 0.243$). We then chose a particular mossy fiber response of the previously-determined class as the source of input to that "dendrite"; we assumed that a "dendrite" is equally likely to choose any of the mossy fibers within a given class. For each synapse, we set the fast and slow components of the synaptic weight by randomly sampling from the pool of all fast+slow weight pairs obtained from fitting the granule cell model to recorded granule cell responses. Finally, if a model granule cell received input from one or more late mossy fibers, we set for each such fiber a probability of that mossy fiber being active after a given command; this probability was drawn from a uniform distribution. This choice was motivated by the observation that the probability of spike firing varied widely across recorded late mossy fibers (unlike the other response classes, which fired after every command).

We then added a spiking threshold V_{thresh} to model cells, measured relative to the average granule cell membrane potential measure before the EOD command, V_{rest}. In model granule cells receiving only early, medium and/or late mossy fiber input, $V_{rest} = E_L$. In model granule cells receiving pause or tonic input, $V_{rest} = E_L + \Sigma_i \bar{r}^i (w^i_{slow} \int \mathcal{E}_{slow}(t)dt + w^i_{fast} \int \mathcal{E}_{fast}(t)dt)$, where $\bar{r}^i$ is the average firing rate of each pause/tonic input. We measured V_{rest} and V_{thresh} in 196 granule cells, and fit the distribution of $V_{thresh} - V_{rest}$ with a Gaussian with $\mu = 20.2$ mV, $\sigma = 5.97$. To set the threshold of model granule cells, we calculated V_{rest} and then sampled granule cell $V_{thresh} = V_{rest} + \mathcal{N}(\mu,\sigma)$, resampling if $V_{thresh} < V_{rest}$. Upon spiking, the cell was clamped to E_L for 4 ms. To simulate the activity of our model granule cell on a single trial, we randomly drew one recorded trial (25 ms before to 200 ms after the EOD command) from each of its presynaptic mossy fibers to be used as input.

Simulating negative image formation. We modeled the medium ganglion cell as a passive, current-based leaky unit receiving excitatory input from 20,000 model granule cells ($r^i(t)$) and sensory input ($s(t)$), with anti-Hebbian spike timing-dependent plasticity at granule cell-medium ganglion cell synapses (w^i), and EPSP (E) fit to granule cell-evoked EPSPs recorded intracellularly in medium ganglion cells[37]. Because the timescale of learning is slow, we assumed the $w^i - s$ to be constant over a single command cycle. $s(t)$ was taken from ref. 1 Figure 1b.

The granule cell- medium ganglion cell learning rule has the form $\mathcal{L}(t) = \Delta^+ - \Delta^- \mathcal{L}_0(t)$ where $t = t_{MGspike} - t_{GCspike}$ and $\mathcal{L}_0(t)$ determines the time dependence of associative depression. Theoretical analysis (**Supplementary Modeling**) has shown that negative images are guaranteed to be stable when $\mathcal{L}_0 = \mathcal{E}$. The timescale of $\mathcal{E}$ agrees learning rules fit to experimental data[3], thus we use $\mathcal{L}_0 = \mathcal{E}$ here. Scaling of the weights by $\mathcal{L}$ was chosen to be multiplicative; because the change in synaptic weights during negative image formation was small, we simply scale $\mathcal{L}$ by the weight before learning ($w^i{}_0$) for each synapse. We set $w^i_0 = (\Sigma_i(\mathcal{E} * r^i)(t^i_{max}))^{-1}$ where $t^i_{max} = \text{argmax}_t(r^i(t))$, which brings the weighted granule cell input to the medium ganglion cell close to constant over time. Thus, with the approximation of linearizing the medium ganglion cell spiking response about the equilibrium voltage V_0 (**Supplementary Modeling**), w^i evolves as $dw^i/d\tau = -w^i_0(\Delta^+ \int r^i(t)dt - \Delta^- \int V(t)(\mathcal{L}_0 * r^i)(t)dt)$, where τ is the period of each EOD cycle.

We fit Δ^+ and Δ^- to negative images recorded experimentally: given experimentally recorded membrane potential changes $\Delta V_{t_D}(t)$ induced by a broad spike at time $t_D \in \{0,25,50,75,100,125,150\}$ ms, and predicted membrane potential change $\Delta\tilde{V}_{t_D}(t) = \Sigma_i w^i_0(\mathcal{E} * r^i)(t)(\Delta^+ \int r^i(s)ds + \Delta^- \int \delta(s - t_D)(\mathcal{L}^0 * r^i)(s)ds)$, we chose Δ^+ and Δ^- to minimize $C(\Delta^+,\Delta^-) = \Sigma_{t_D} \min_{c_{t_D}} \int(\Delta V_{t_D}(t) - \Delta\tilde{V}_{t_D}(t) + c_{t_D})^2 dt$ using standard linear least-squares, where c_{t_D} is a constant offset term used to remove the effect of any net drift in membrane potential.

To monitor the degree of negative image formation during simulation, given a total change to each weight, Δw^i, we defined the residual signal error as $(\int(s(t) + \Delta w^i(\mathcal{E} * r^i)(t))^2 dt)/\int s(t)^2 dt$.

35. Rancz, E.A. *et al.* High-fidelity transmission of sensory information by single cerebellar mossy fibre boutons. *Nature* **450**, 1245–1248 (2007).
36. Efron, B., Hastie, T., Johnstone, I. & Tibshirani, R. Least angle regression. *Ann. Stat.* **32**, 407–451 (2004).
37. Grant, K., Sugawara, S., Gomez, L., Han, V.Z. & Bell, C.C. The mormyrid electrosensory lobe *in vitro*: physiology and pharmacology of cells and circuits. *J. Neurosci.* **18**, 6009–6025 (1998).

doi:10.1038/nn.3650